Damage in Armor Ceramics Subjected to High-Strain-Rate Dynamic Loadings: The Edge-On Impact Test

Pascal Forquin, Antonio Cosculluela

HAL Id: hal-04470396

https://hal.univ-grenoble-alpes.fr/hal-04470396v1

Submitted on 4 Mar 2024

DAMAGE IN ARMOR CERAMICS SUBJECTED TO HIGH-STRAIN-RATE DYNAMIC LOADINGS. THE EDGE-ON IMPACT TEST

Pascal Forquin[1]*, Antonio Cosculluela[2]

[1]Univ. Grenoble Alpes, Grenoble INP, CNRS, Laboratoire 3SR, BP53, 38041 Grenoble cedex 9, France, pascal.forquin@3sr-grenoble.fr

[2]CEA-CESTA, 15 avenue des Sablières, CS 60001, 33116 Le Barp Cedex 1, France, antonio.cosculluela@cea.fr

*Corresponding author

Abstract

The objective of this chapter devoted to "Damage in armor ceramics subjected to high-strain-rate dynamic loadings" is dedicated to the Edge-On-Impact testing technique. This experimental method is commonly used to investigate the high strain-rate tensile damage induced in armor ceramics when subjected to impact loading. The principle of EOI test is the following: a metallic cylindrical projectile hits the edge of a rectangular tile which thickness is generally smaller than the projectile diameter. The compressive strength of ceramics being much higher than their tensile strength, tensile damage occurs without inducing any compressive damage near the impact point. This anisotropic damage, called multiple-fragmentation process, is composed of a large number of oriented cracks. Two testing configurations are generally considered. In the so-called open configuration an ultra-high-speed camera is used to visualize the fragmentation process as function of time. In the sarcophagus configuration, a metallic or polymeric casing is used to keep the fragments in place so the damage pattern can be analyzed further by microscopy or X-ray micro-tomography analysis. Next the damage pattern can be compared to numerical predictions. In this chapter, a short review of experimental works proposed in the literature based on the use of EOI tests is presented. A numerical study is introduced to assess the loading history and loading-rate involved in such test. Next, experimental results conducted with 4 silicon carbide ceramics are presented. Finally, these experiments are numerically simulated in a FE code with the DFH (Denoual-Forquin-Hild) anisotropic damage model and the final damage patterns are compared to post-mortem observation in terms of cracking density. Last, the strengths, weaknesses and drawbacks of EOI tests are discussed.

Keywords: Impact tests, Multiple fragmentation, Ceramics, Tensile damage, Cracking density, Armor, Dynamic behavior

1 Introduction: why tensile damage in armor ceramics needs to be investigated?

During a ballistic impact, complex successive loadings develop leading to extensive damage modes within the ceramic plate (den Reijer 1991; Cosculluela 1992; Forquin 2003; Normandia et al. 2004; Chen et al. 2007; Zinszner 2014). In the first microseconds, high pressures are supposed to induce microplasticity and micro-damage mechanisms into the ceramic (Cagnoux and Cosculluela 1991) and also the fracture of the projectile's core. However, during the second step, tensile stresses develop in the whole ceramic plate leading to an intense fragmentation process in the material composed of a high density of oriented cracks triggered on pre-existing flaws (Forquin et al. 2003). Finally, in the third and last step, the (broken) projectile penetrates into the comminuted ceramic target. In that stage, the behavior of the fragmented ceramic may have a strong influence on the penetration resistance of the protective armor system. According to Krell and Strassburger (2014), the top priority factor driving armour ballistic performance is the ceramic fragmentation. It is the reason why this tensile damage needs to be investigated and numerically simulated. For instance, the tensile damage induced under normal impact is investigated by (Riou 1996) considering a bi-layer target, composed of a front plate 20 mm thick made of silicon carbide and a steel rear plate, which is subjected to the ballistic impact of a cylindrical projectile (11 mm in diameter, 100C6 steel) considering an impact velocity of 250 m/s (Fig. 1). In this configuration, the compression stresses generated in the ceramic tile are not high enough to induce any compression damage and plastic deformation. However, in weak of the longitudinal incident wave tensile stresses develop at high strain-rates leading to an intense fragmentation process within the target. The ceramic plate is infiltrated with a hyperfluid resin and a cut view of the target is shown in the Figure 1. A tensile damage that consists of cracks of millimeter size spaced from about 200 to 500 μm is observed. The damage pattern is composed of "Hertz cracks" initiated near the front surface and "radial cracks" within the bulk of the plate. In addition, "release cracks" are initiated on the rear face of the ceramic tile due to the reflection of the waves at the ceramic-backing interface. Furthermore, "spall cracks" parallel to the front and rear faces are detected resulting, a priori, from the crossing of release waves in the bulk of ceramic plate. This tensile damage is difficult to observe in the case of the ballistic impact of an armor-piercing projectile due to the penetration process and the ejection of debris. However, thanks to EOI experiments instrumented with ultra-high-speed photography, it is known that tensile damage develops in a few microseconds and precedes the penetration stage. Therefore, tensile damage in armor ceramics needs to be investigated and the role or microstructure needs to be understood. In particular, the distribution of the critical flaws from which cracks are triggered has to be determined and implemented in an analytical or numerical modeling of the fragmentation process, which needs to be validated (Forquin et al 2021). To do so, the EOI testing method may constitute a convenient and easy experimental method. A short review of existing experimental works is presented in the next subsection. Next, a numerical study of an EOI tests is introduced. Experimental results obtained with four grades of SiC are presented in the last subsection of this chapter.
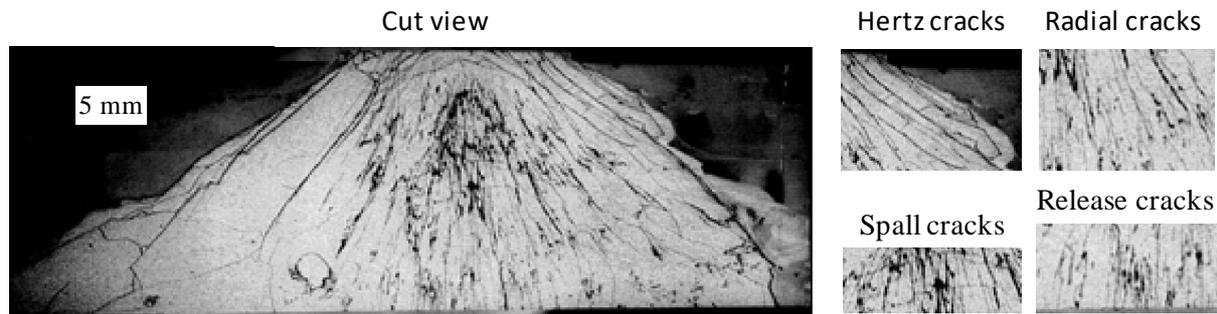
Cut view   Hertz cracks   Radial cracks

Spall cracks   Release cracks

Fig. 1 Cut view of a SiC ceramic plate impacted with a steel cylindrical projectile at an impact speed of 250 m/s (Riou 1996)

2 The Edge-On Impact testing technique: a short review

The edge-on impact testing technic constitutes one of the most efficient and easiest experimental methods to investigate and to visualize the growth of tensile damage induced in brittle solids when subjected to high-strain rates. This method was pioneered, almost simultaneously, by Strassburger and coworkers in EMI (Ernest-Mach-Institute) (Strassburger and Senf 1995; Senf et al. 1994) and by Riou and coworkers in CTA (Centre Technique d'Arcueil, DGA) (Riou 1996; Riou et al. 1998a; Denoual and Hild 2000; Forquin et al. 2003). It consists in the impact of a cylindrical projectile against one of the edges of the tested ceramic tile. The projectile is usually larger in diameter than the target thickness and much smaller than the target height. It results in an impulsive loading characterized by a very short rising time (less than 1 μs). The loading, of triaxial shape in the vicinity of the contact area, turns into a bi-dimensional (plane stress) divergent wave propagating in the whole target. It is the reason why the stress amplitude is expected to decline more slowly (in $1/\sqrt{r}$) compared to a spherical expansion for which a decrease in $(1/r)$ is observed. Accordingly, damage develops much further in distance which facilitates the observations with high-speed imaging system. Thus, in the so-called open-configuration the lateral face of the target is visualized thanks to ultra-high-speed photography equipment used at frame-rates usually set from 2 μs down to 0.1 μs. In this configuration, the camera is installed along the axis of the light reflection of the incident light provided by a flash unit or continuous light unit. The visualized surface is usually polished to increase the amount of light captured by the camera but also to improve the observation of cracks by contrast.

This experimental method provides several advantages compared to other testing techniques. For instance, Brazilian tests performed with Split Hokinson Pressure Bar apparatus are limited to much lower strain-rates (about a few tens of s⁻¹) when applied to ceramics. The limited loading-rate results from long rising time of loading (above 20 μs) that needs to be applied to the sample to ensure a correct mechanical balance. For instance, typical stress-rates ranging from 3 to 6 MPa.μs⁻¹ are obtained in Brazilian tests applied to alumina samples in Galvez et al. (1997), Chen et al. (2014) and in Scapin et al. (2017) leading to a single fracture in each tested specimen. On the other hand, in edge-on impact experiments, typical strain-rates ranging from few thousands of s⁻¹ to a few tens of thousands of s⁻¹ are generated (Forquin et al. 2018), leading to an intense multiple fragmentation process in the target.

In contrast, the spalling testing method by shockless plate-impact (Dargand and Forquin, 2021) or by pulsed-power technology provides the advantage of a direct measurement of the spall strength (Zinszner et al. 2015a; Zinszner et al. 2017) and provides much higher strain-rates (mostly above 10^4 s^{-1}). However, the spall fracture is hidden in the bulk of the sample and cannot be visualized by high-speed photography. In addition, the fracture pattern remains difficult to analyze through post-mortem observations. The edge-on impact testing technique requires also much less costly gas gun facility compared to those used for plate-impact tests, which operates with a larger caliber and under vacuum, or compared to pulsed power generator facilities.

Different dimensions of projectiles, impacted plates and impacting velocities have been considered in the literature. For instance, ceramic plates 100 x 100 x 10 mm^3 were impacted with steel cylinders of 30 mm diameter and 23 mm in length with impact velocities ranging from 50 to 1000 m/s in (Senf et al. 1994), (Strassburger and Senf 1995). The damage formation was visualized by means of high-speed Cranz-Schardin film camera during the first 12 µs after projectile impact. Experiments performed with glass and SiC ceramics (Brajer et al. 2003; Strassburger 2004) and more recently with boron carbide (B4C) ceramic (Strassburger et al. 2013) were used to characterize the so-called Damage velocity (velocity of the damage front), the Cone crack velocity and the Secondary crack velocity (cracks initiated by the shear wave travelling along the impacted edge of the specimen) as function of the Impact velocity.

In the experiments performed by Riou (1996) and by Riou et al. (1998a; 1998b) a hard-steel cylinder projectile (D11H20) impacts the edge of a dense natural sintered α Silicon Carbide at an impact velocity ranging from 100 to 300 m/s. The ceramic tile is backed or not with a steel confinement beam. The beam dimensions are 100 mm x 10 mm x T with a thickness T equal to 15 or 20 mm. A schematic of the test configuration is given in Fig. 2a. Two pictures taken 2.9 µs after impact with an Imacon 790 high-speed camera are shown in the Figures 2b and 2c. In the first picture (Fig. 2b) a SiC beam sample is subjected to the impact of a projectile at an impact speed of 250 m/s. In the second test (Fig. 2c), the SiC target is constrained on its back with a steel beam and is impacted roughly at the same impact speed (260 m/s). A damage pattern composed of a large number of oriented short cracks is observed in less than 3 µs. It is concluded by the authors that the back-steel confinement seems to not interfere with initial damage shape generated in the first 3 µs whereas the presence of the confinement seems to limit the initiation of transverse (spall) cracks in the two next µs.
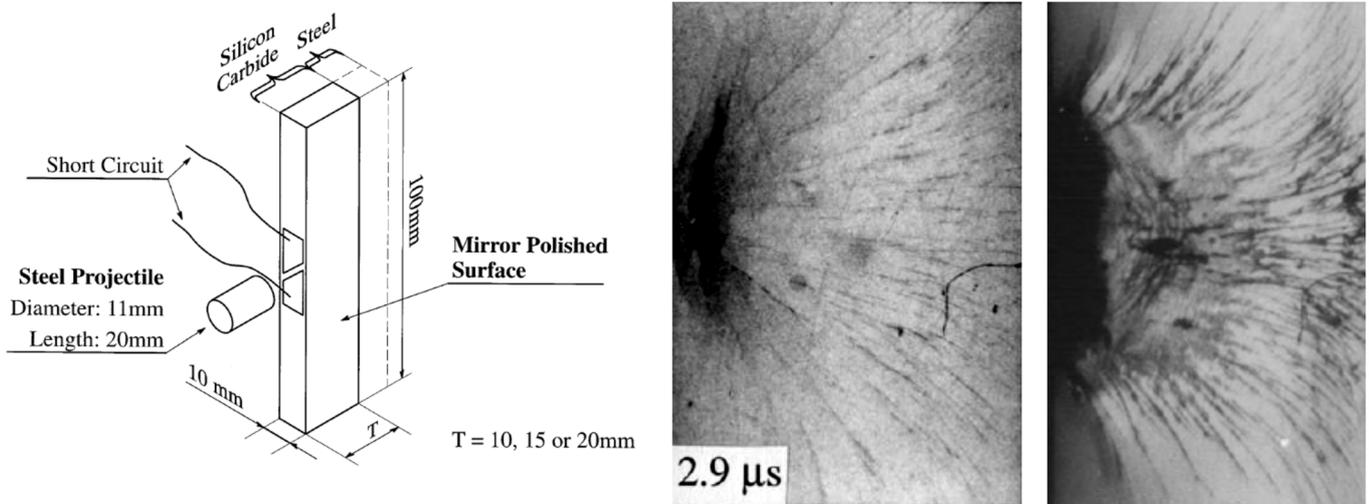
Fig. 2 Edge-on impact experiments performed by (Riou et al. 1998a). (a) Experimental set-up, (b) and (c) Damage at 2.9 μs, (b) Unconfined 15 mm thick SiC target impacted at 250 m/s, (c) Back steel confined 15 mm thick SiC target impacted at 260 m/s

The fragmentation process induced in a porous SiC ceramic filled or not with an aluminum alloy though its open porosity was investigated in (Forquin et al. 2003) by means of EOI tests in open configuration (use of a high-speed camera) and in sarcophagus configuration. This last configuration is depicted on the Figure 3a. It is composed of a metallic casing made of aluminum alloy that surrounds the ceramic tile with the aim to keep the fragments in place. However, small paper wedges are placed in-between the ceramic tile and the aluminum casing to ensure an impedance discontinuity. It is the reason why, the same number of cracks is expected for both (open and sarcophagus) configurations. After impact, the fragmented ceramic tiles were infiltrated in the sarcophagus with a hyper fluid resin (Epoxy, Struers) and then polished for optical observations as shown in Figures 3b, 3c and 3d. The tests conducted at 100 m/s and 200 m/s revealed an increase of the cracking density in R-SiC ceramic with the increase of loading-rate. The test performed at an impact speed of 200 m/s with the infiltrated ceramic showed a decrease of the intensity of fragmentation compared to the non-infiltrated ceramic and a very good residual strength. The fragmentation process was simulated with a finite-element code considering the DFH (Denoual-Forquin-Hild) anisotropic damage model along with Weibull parameters identified from bending tests. The experimental and numerical results demonstrated that the aluminum alloy infiltrated through the open porosity of the ceramic results in two beneficial effects: on the one hand it increases the crack-inception stresses lowering the cracking density. On the other hand it creates a bridging effect leading to a much higher residual strength of the fragmented targets. Both effects are seen to be beneficial regarding a multi-hit loading scenario.
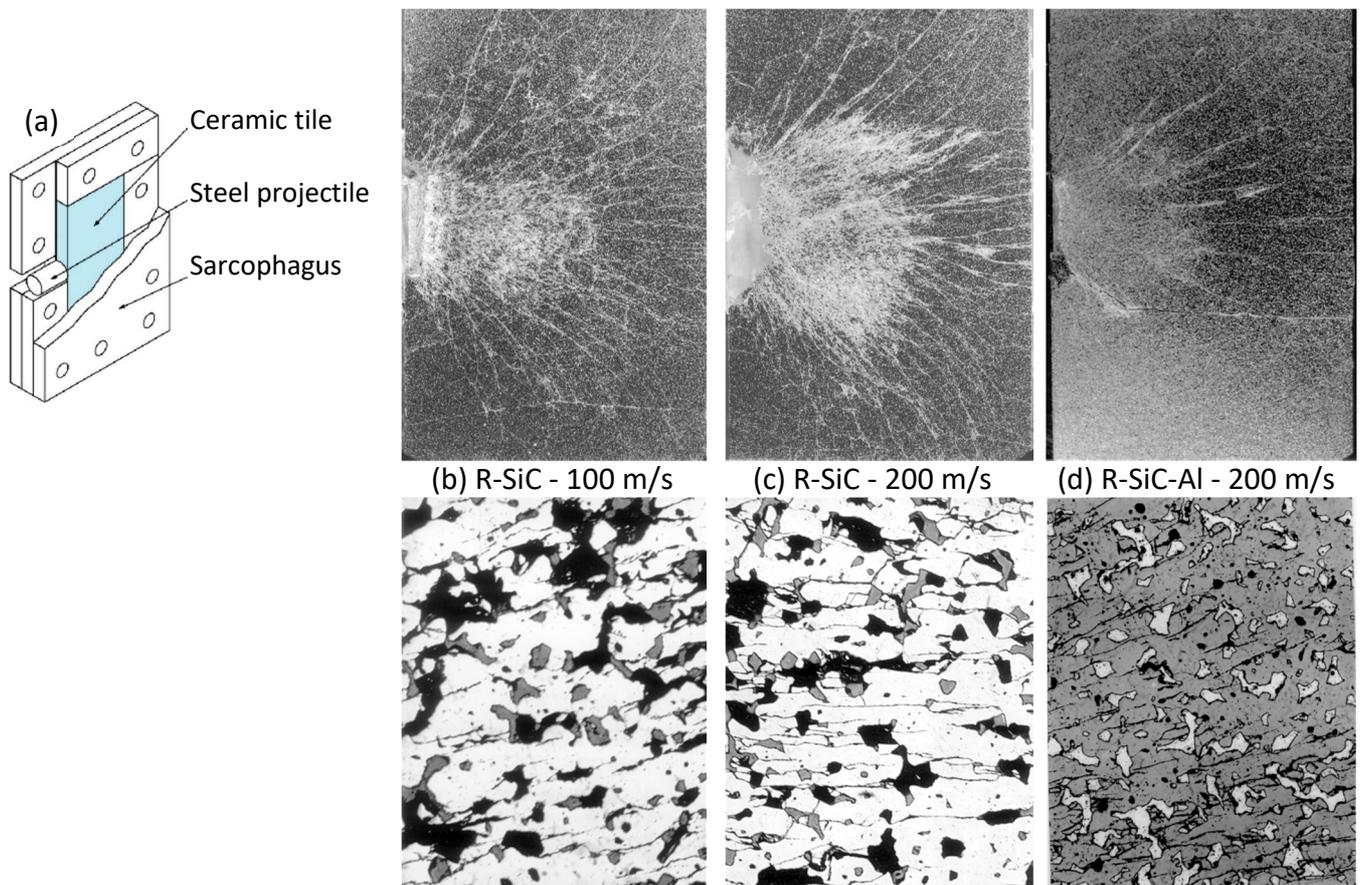
Fig. 3 Edge-on impact experiments performed in (Forquin et al 2003). (a) Sarcophagus configuration, (b) R-SiC target impacted at 100 m/s, (c) R-SiC target impacted at 200 m/s, (d) R-SiC-Al target impacted at 200 m/s

In the work developed in (Riedel et al 2010), the elastic stress histories involved in an EOI test was numerically investigated and compared to those involved in a depth-of-penetration (DOP) test configuration and planar plate impact (PPI) experiments. In addition, the fracture processes in the target was numerically simulated with a mesh-free SPH code. It is concluded that an anisotropic damage representation along with tensile stress failure criteria are requested to represent the damage propagation produced by diverging shock waves.

In the work conducted in (Leavy 2013) the EOI technique was used as benchmark to validate ceramic constitutive models implemented in a dynamic simulation code. To do so, a Weibull distribution is introduced in a hydrostatic tension criterion for describing the variability of material strength and the numerical predictions in terms of damage velocity versus impact velocity were compared to experimental observations provided by high speed photography.

More recently, the edge-on impact technics was extended to the investigation of the fracturing process in transparent armor ceramics such as single crystal (sapphire) and AlON (spinel) polycrystalline ceramics (McCauley et al. 2013). The kinetics of damage and fracturing features in transparent ZnS ceramic and in sapphire single crystal was more recently analyzed in (Forquin 2016) and in (Forquin and Zinszner 2017). In the experiments reported in Figure 4, monocrystalline sapphire ceramic targets of size 60x60x4 mm^3

are impacted on the edge with a cylindrical projectile 10 mm in diameter at an impact speed about 230 m/s. As illustrated by the pictures of Kirana ultra-high speed camera the fragmentation process develops in a ten of microseconds. It is observed that cracks propagate following specific orientations in relation to the C axis direction.
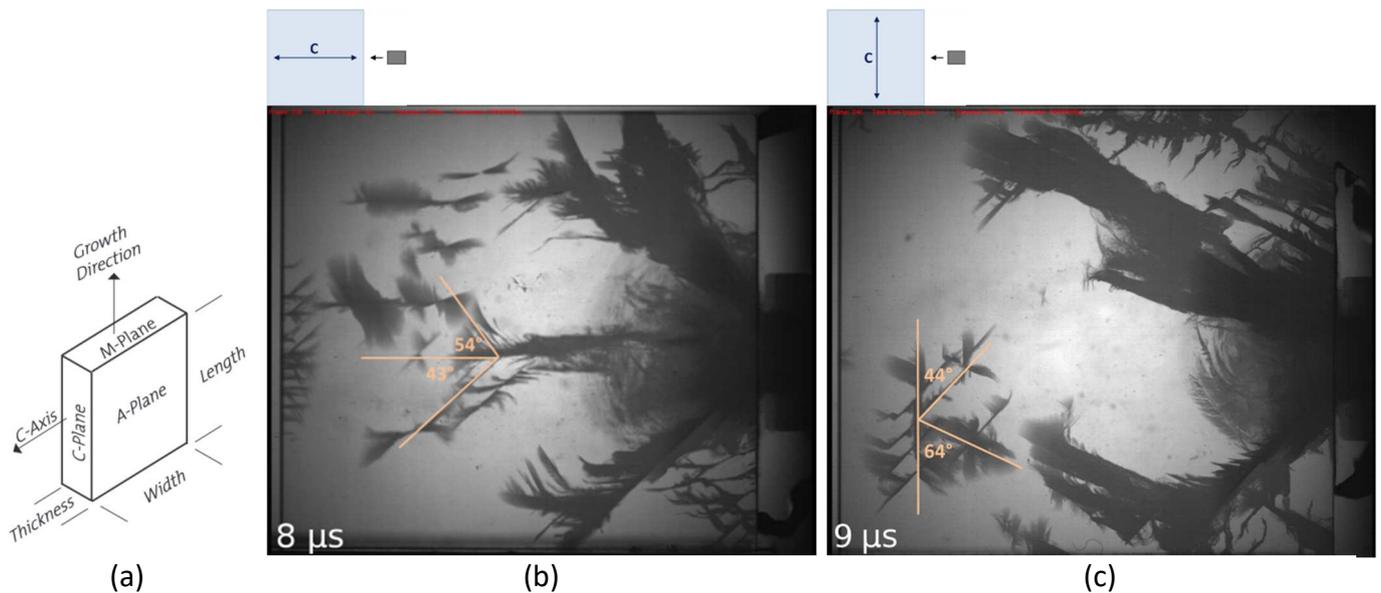

Fig. 4 Edge-on impact experiments performed against sapphire single crystal at an impact speed around 230 m/s (Forquin and Zinszner 2017). (a) Sapphire single crystal orientation (Saint-Gobain doc.). (b) Impact direction parallel to the C axis (horizontal axis). (c) Impact direction orthogonal to the C axis (vertical axis).

The intergranular and transgranular fracturing observed in polycrystalline AlON transparent ceramics subjected to EOI tests in (McCauley et al. 2013) was numerically simulated by (Zhang et al. 2018) considering a peridynamics numerical method. For this purpose, a model in which individual grains are represented was built. This numerical approach allows describing the primary failure front that grows at intersonic (supershear) propagation speed as well as the localized cracks which develops at sub-Rayleigh propagation speed.

The EOI experiments conducted on AlON in (Strassburger 2004; Strassburger et al. 2005; 2006) were analyzed and modeled in (Tonge and Ramesh 2016) by considering a micromechanics-based model in order to describe the damage growth, the deviatoric and volumetric granular flow and pore compaction mechanisms that develop preferentially in the interior of the plate rather than on the surface due to inertial confinement. Again, the flaw distribution is observed to be an important parameter to account for the role of microstructure on the damage process.

In conclusion, the edge-on impact testing configuration has been used extensively for the last three decades to explore the fragmentation process in different kinds of ceramic armors. The high-speed photography has revealed several features of the fragmentation process generated in these materials under impact loading. In particular, it is observed that the fragmentation process is composed of a high number of cracks oriented perpendicularly to the positive principle stress. A numerical investigation of

the loading history is presented thereafter. Next, a comparison of the fragmentation properties of 4 SiC ceramics is proposed.

3   *Numerical investigation of an edge-on impact test*

The mechanical loading involved in an edge-on impact experiment was investigated in (Forquin et al. 2018) by means of numerical simulations conducted with the commercial Abaqus-Explicit Finite Element code. The considered target is a silicon carbide plate 60 x 30 x 8 mm^3 impacted with a cylindrical projectile (D10 x H15) at a striking velocity of 175 m/s. These numerical simulations aim to estimate the level of loading-rate leading to to the ceramic fragmentation. For this purpose, an isotropic elastic behavior is considered for the ceramic with a Young's modulus E = 410 GPa and a Poisson's ratio v = 0.14. A mesh made of "C3D8R" eight-node solid brick elements with reduced integration is considered for the projectile and target with a mesh size of approximately 1 mm. An elastic-perfectly-plastic model is used for the projectile with a yield stress of Y = 1300 MPa. Two symmetry planes are considered so a quarter of the projectile-target configuration is meshed. The field of hoop stresses at 1, 2 and 3 μs after impact is depicted on the Figure 5 with a cylindrical coordinate system ($\vec{e}_r$, $\vec{e}_\theta$, $\vec{e}_z$) centered at the initial point of impact. Tensile stresses are observed at 7 mm (t = 1 μs) and 15 mm (t = 2 μs) from the initial point of impact and at t = 3 μs near the target rear edge. The strain-rate level in finite-elements located along the impact axis at a distance of 10 and 20 mm from the initial impact point was estimated. It is about 7750 s^{-1} and 1850 s^{-1} respectively at 10 and 20 mm (Figure 6).
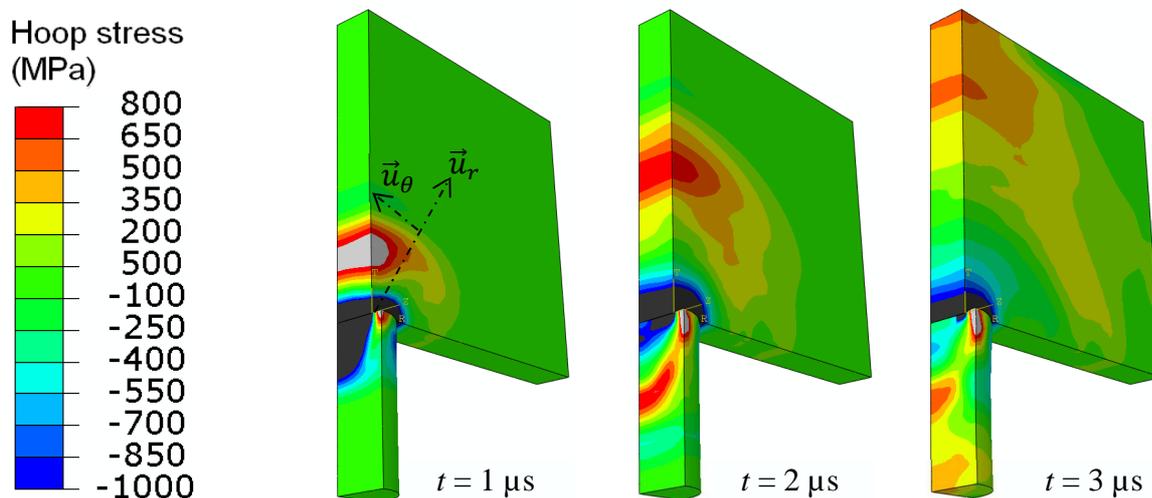

Fig. 5 Numerical simulation of edge-on impact experiments with a striking velocity of 175 m/s using an elastic model for the ceramic target
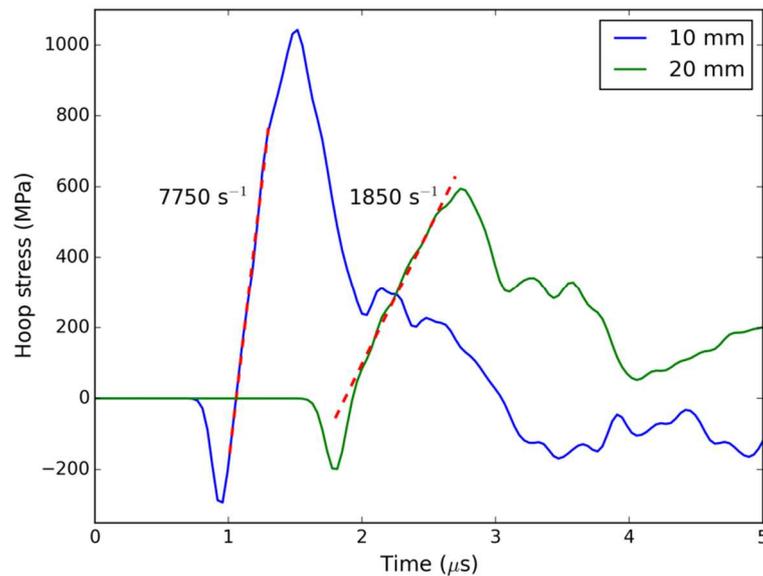
Fig. 6 Profile of the hoop stress as a function of time in edge-on impact experiments at 10 and 20 mm toward the initial impact point, and an estimation of the strain-rate

4   Experiments conducted on silicon carbide ceramics

4.1 Presentation of the SiC ceramics

The edge-on impact testing method was applied to four SiC ceramics of different microstructures in (Rossiquet 2012; Zinszner 2014; Forquin et al. 2018). The first grade, referred as 'PS-S' (Pressure-less Sintered in Solid state) corresponds to a commercial product of Saint-Gobain also named Hexoloy SA®. It is performed in pressure-less solid state sintering at 2150°C. Its density corresponds to 98% of the theoretical density and its microstructure is characterized by fine and equiaxed grains about 4 to 10 μm (Figure 7a). The SPS (Spark Plasma Sintered in Solid state) SiC ceramic is produced in solid-state sintering at 2000°C for 5 minutes under a 40 MPa compaction pressure.) and is called 'SPS-S'. The resulting microstructure for this grade shows elongated grains, 100 μm in length, distributed among smaller and more equiaxed grains (Figure 7b). Its density reaches around 99% of the theoretical one. The third grade referred to as 'PS-L' is sintered in pressure-less condition and in liquid phase state at 1875°C for 30 minutes under argon. Its microstructure exhibits equiaxed grains of average grain size around 3 μm surrounded by a secondary phase which is mainly composed of YAG ($Y_3Al_5O_{12}$) (Figure 7c). Its density corresponds to 98% of the theoretical density. The last SiC grade called 'SPS-L' (Spark Plasma Sintering in Liquid state) is sintered in liquid phase state by SPS at 2050°C for 15 minutes under a 40 MPa. Its microstructure is characterized by a equiaxed grains submicron grains of average size about 500 nm bounded by an amorphous secondary phase made of Al and Y as shown in the Figure 7d. The measured density reaches 98.5% of the theoretical density. Several basic properties of each ceramic are listed in the Table 1. The experimental results obtained with each SiC grade are reported in the next subsection.
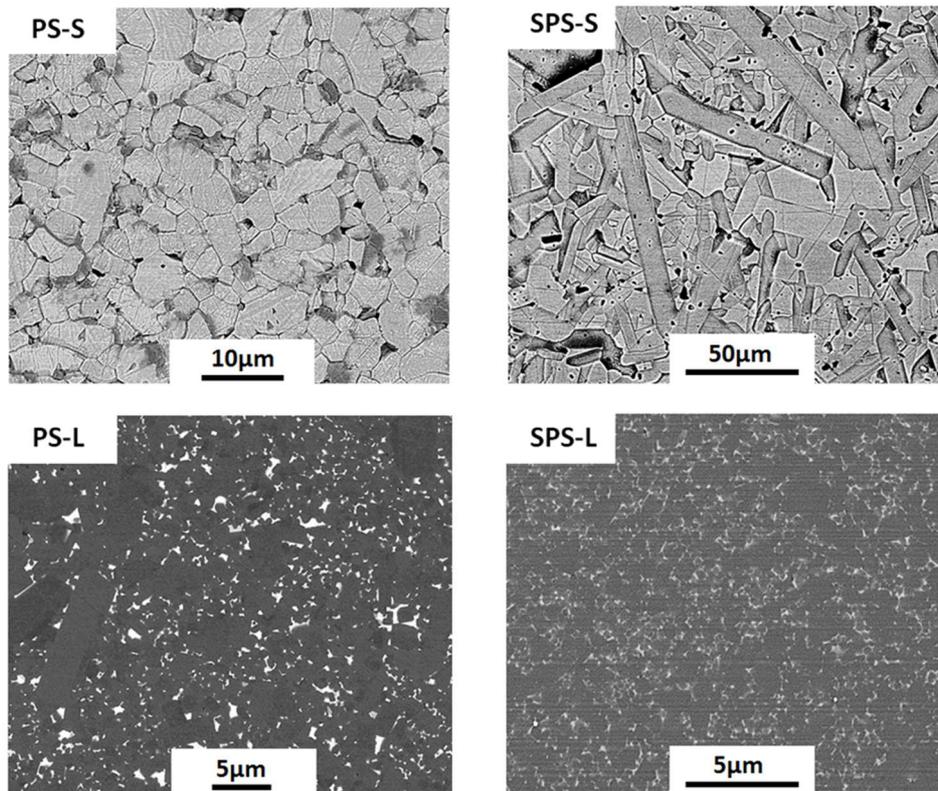
Fig. 7 SEM images of microstructures from grades a) PS-S, b) SPS-S, c) PS-L and d) SPS-L after mirror polishing (Rossiquet 2012). Samples a) and b) have been chemically etched in order to reveal microstructures. Samples c) and d) have not been etched since the contrast between SiC grains and secondary phases allows an easy observation of the microstructures

Table 1 Main sintering and mechanical properties of the four SiC grades (Rossiquet 2012; Zinszner 2014)

SiC grade	Sintering process	Sintering phase state	Sintering additives	Average grain size (μm)	Hardness H_{V1} (GPa)	Density (kg/m^3)	Toughness (MPa√m)
PS-S	Pressure-less	Solid	$B_4C + C$	6	24.3	3150	3.0
SPS-S	SPS	Solid	$B_4C + C$	/	27.0	3170	2.5
PS-L	Pressure-less	Liquid	YAG	3	22.2	3260	5.2
SPS-L	SPS	Liquid	YAG	0.5	23.9	3210	3.8

4.2 Experimental set-up and instrumentation

Edge-on impact tests are performed in 'open configuration' and in a 'sarcophagus configuration' with cylindrical projectile 10 mm in diameter, and 15 mm in length made of high strength steel (elastic limit: 1300 MPa). The specimen is 60 mm in length, 8 mm thick, and the visualized side is 60 x 30 mm². The impact velocity is approximately 170±5 m/s. In the open configuration, the ceramic tile is free with no

casing. An aluminum casing is used in the sarcophagus configuration to keep most of the fragments in place. In addition, small paper wedges are inserted in-between the ceramic plate and the metallic casing to ensure an impedance discontinuity, so the expected number of cracks in both (open and sarcophagus) configurations is the same.
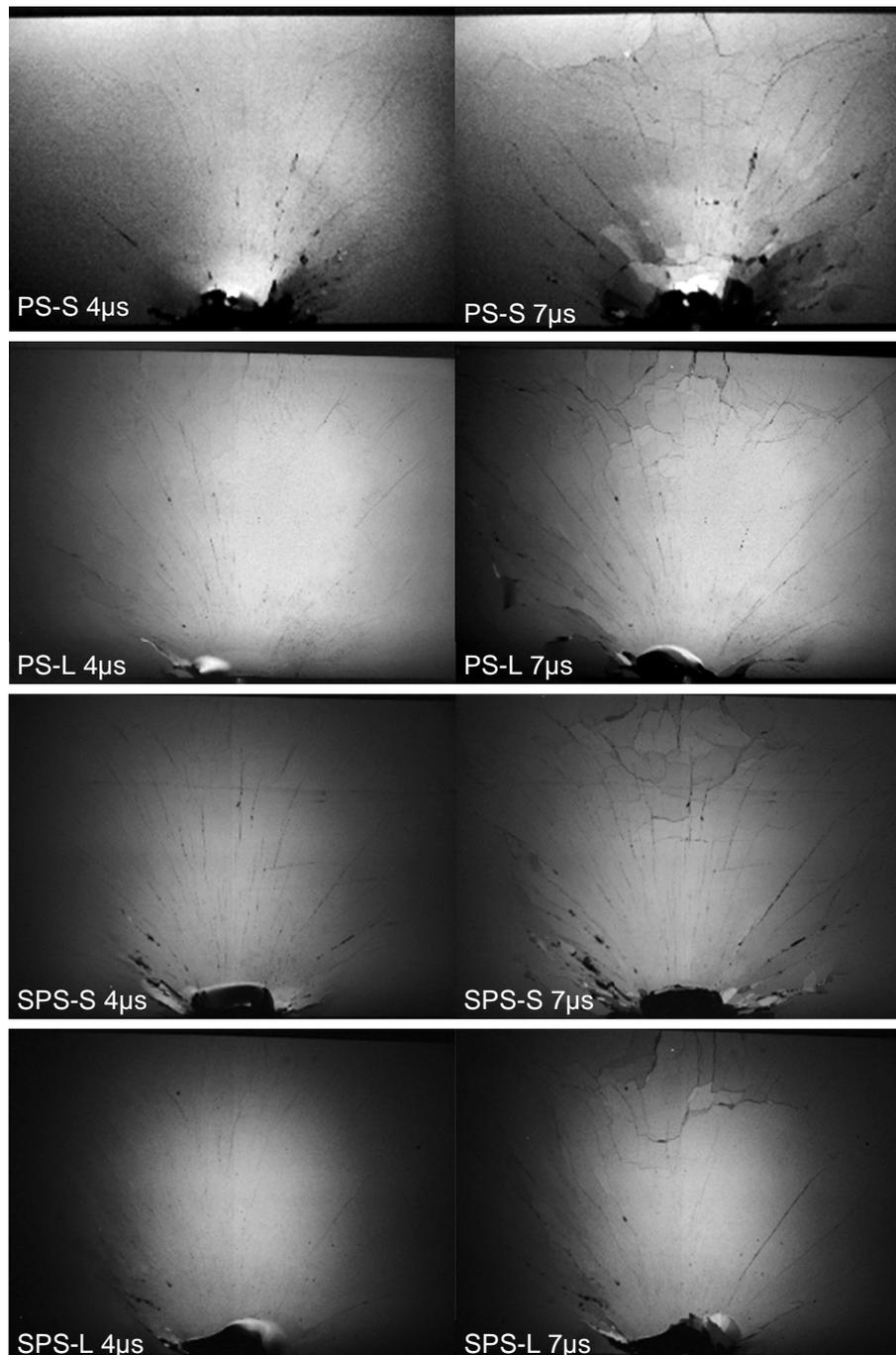
4.3 Experimental results obtained in open-configuration

Fig. 8 Images at t = 4 and 7 μs of EOI tests performed with 4 SiC ceramics. The striking velocity is 181, 169, 170, 172 m/s for PS-S, PS-L, SPS-S, SPS-L targets, respectively (Forquin et al. 2018)

In open configuration EOI experiments are performed with an ultra-high-speed camera (Shimadzu HPV-1) with an inter-frame time set to 1 μs in order to visualize the growth of the fragmentation during impact. A velocity interferometer pointed out to the ceramic rear edge is used to trig the camera. The fragmentation pattern of each ceramic tile is depicted in the Figure 8 at 4 and 7 μs after impact. In the first 4 μs "radial cracks" initiates and develops within the whole target and "release cracks" are triggered at the rear edge of the target. At t = 7 μs, cracks initiate perpendicularly to the radial cracks, so the target is completely damaged. The cracking density appears to be clearly smaller in PS-L and SPS-L ceramic grades compared to the PS-S and the SPS-S grades, which confirms the influence of microstructure on the fragmentation process.

4.4 Experimental results obtained in in sarcophagus-configuration

Edge-on impact experiments in sarcophagus configuration were conducted with the four SiC ceramics as detailed in (Forquin et al. 2018). The impacted targets were infiltrated post-test with a hyper fluid Epoxy resin before polishing for optical observations. Different set of cracks are observed in Figure 9.
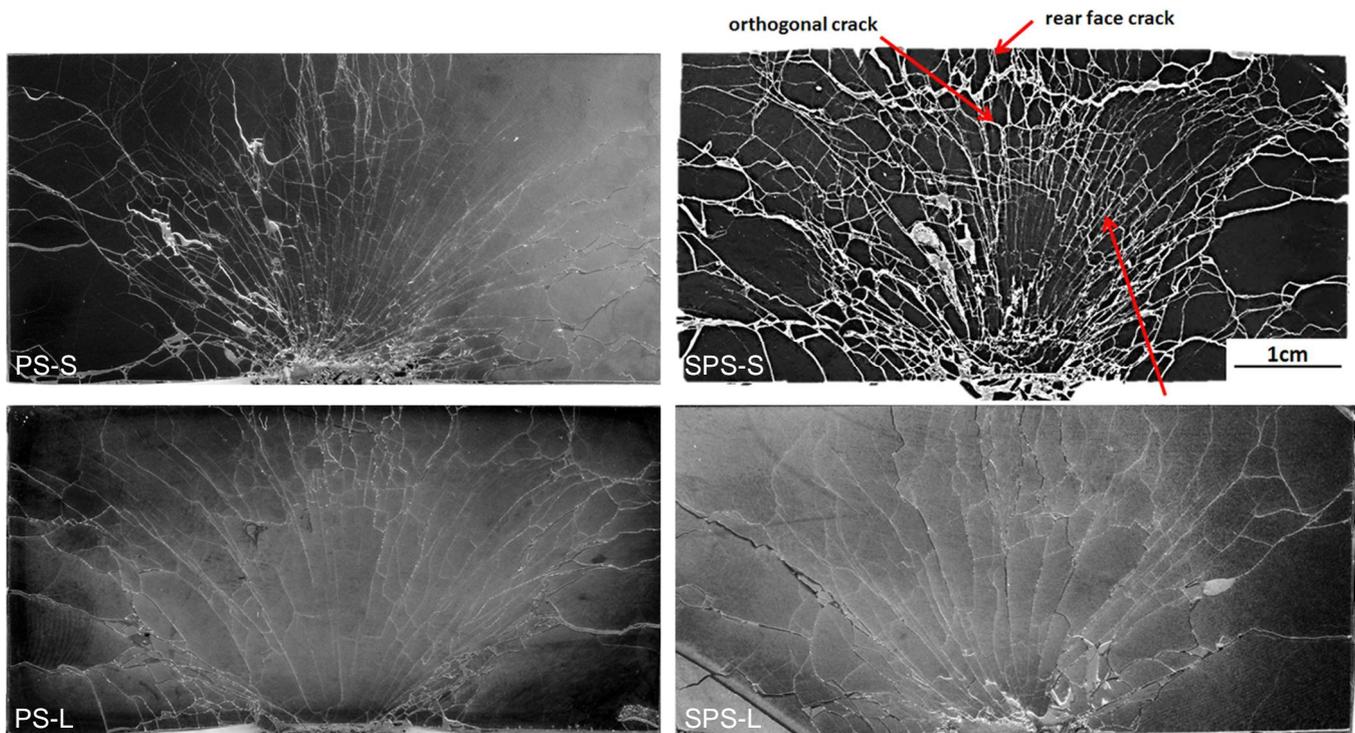

Fig. 9 Post-mortem damage patterns for four impacted SiC tiles in the sarcophagus configuration. The striking velocity is 166, 175, 165, 174 m/s for PS-S, PS-L, SPS-S, SPS-L targets, respectively (Forquin et al. 2018)

Numerous radial cracks are observed as already noted in the high-speed camera images. So-called "Conical cracks" initiate on the impacted edge of the target. Cracks initiate at the rear edge of the target due to release waves. Last, a few cracks propagate perpendicularly to the radial cracks in the center of the target. The crack density (λ_{cracks}) is estimated at about 10 mm from the initial impact point for each grade by considering the mean distance (d_{cracks}) between parallel cracks according to the formula: λ_{cracks} = $1/(d_{cracks})^3$ (Forquin et al. 2018). In PS-S grade, the mean distance between cracks 0.21 mm corresponds

to a crack density of 1.0×10^{11} cracks/m³. In SPS-S grade, the estimated crack density at 10 mm from the initial impact point is about 7.3×10^{10} cracks/m³. In PS-L and SPS-L grades the crack density is significantly and is about 7.6×10^9 cracks/m³ and 4.2×10^9 cracks/m³ respectively in the PS-L and SPS-L grades.

4.5 Tomographic analysis of fragments

The infiltrated targets of two SiC grades (SPS-L and SPS-S) are scanned using the micro-x-ray tomography machine in 3SR Laboratory. In this setup, a micro-focus x-ray beam generates a polychromatic cone beam (generated with a 150 kV and 200 µA electron beam against a Tungsten target) which is detected by a flat panel detector with 1536x1920 pixels each measuring 0.127x0.127 mm. The distance between the source and the detector is 767 mm.

The sample is placed on a rotation stage so the sample is X-rayed by considering 1440 angles spread out equally over 360°. At each angle, 8 radiographs are acquired and averaged together to reduce noise. Between each angle a small dithering motion is applied to the detector to avoid ring-artefacts. The impacted target is set in-between the source and the screen at a position resulting in a pixel size of 40 µm/px.

In the work proposed by (Forquin and Ando 2017) a processing of images was developed to analyze the fragments size distribution. For this purpose, cracks in the matrix are first identified. If crack opening exceeds 40 µm the greyscale value inside the crack is constant and corresponds to the value of the resin. However, when crack opening is smaller than 40 µm the traces on the grey-levels are faint and the cracks are detected from a local measurement of gradient. To do so, 3D Sobel operator (gradient filter typically used for edge-detection) is used. After thresholding, a 3D binary image is obtained providing a good identification of cracks opened of less than or equal to one pixel. Next, the binary image is separated into individual particles by calculating the Euclidean Distance Map of the solid phase, whose maxima are used as seed points in a markers-based watershed on the Euclidean Distance Map (Jeon et al. 2004). This analysis was applied to two scanned samples (SPS-L and SPS-S SiC grades). The 3D rendered labelled images and crack networks are depicted in the Figure 10. Starting from the final labelled images, the volume in voxels of each individual particle is measured and converted into a physical volume (in µm³) given the volume of one voxel: 40x40x40 µm³.

Finally, the fragments size distribution is compared to results from physical sieving on similar specimens. The obtained particle size distributions and those obtained from post-mortem sieves of the fragments of other tests on the same materials (SPS-L and SPS-S) (Rossiquet 2012) are shown in the Figure 10, the results obtained with both technics appear to match quite well. In addition, the Weibull and Rosin-Rammler distribution model: $y = 1 - \exp\left(-\left(\frac{x}{x_0}\right)^m\right)$ was considered to identify a size distribution function. The corresponding values of m that describes the spread of the distribution are reported on the Figure 11. In conclusion, the X-ray tomography analyses developed in (Forquin and Ando 2017) confirms that, depending on the initial microstructure of SiC ceramics, strong differences can be observed regarding their final fragmentation properties and final damage pattern when subjected to the same impact loading. This conclusion was recently extended to dense and nacre-like alumina ceramics which fragmentation pattern was analyzed through tomographic analysis after a normal impact test (Duplan and Forquin, 2021). In addition, their post-fragmentation behavior was investigated by means of tandem impact experiments which consist to perform a penetrating impact against the fragmented ceramic backed with

an aluminum plate. These experiments illustrated the effect of fragments size, orientation and anisotropy on the penetrating resistance of the fragmented ceramics.
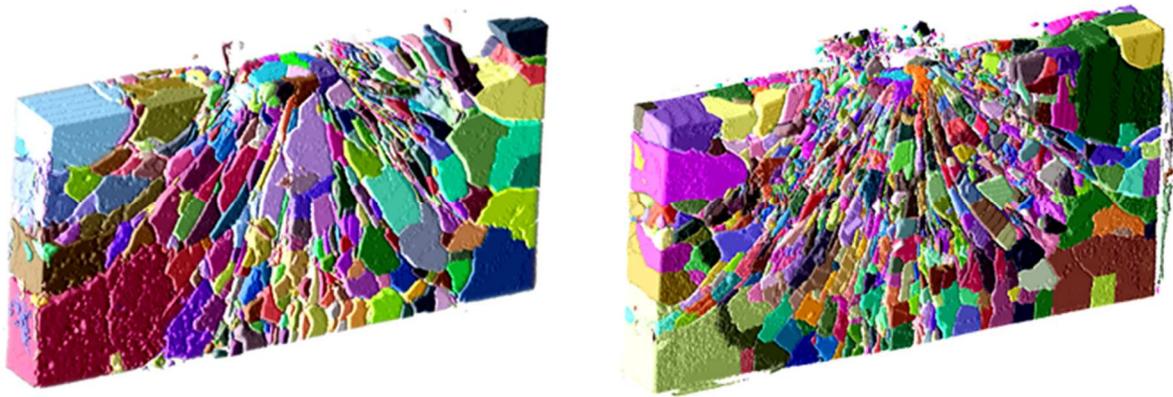

Fig. 10 Particle 3D rendering provided by the fragment labelling procedure developed in (Forquin and Ando 2017). Left: SPS-L, right: SPS-S
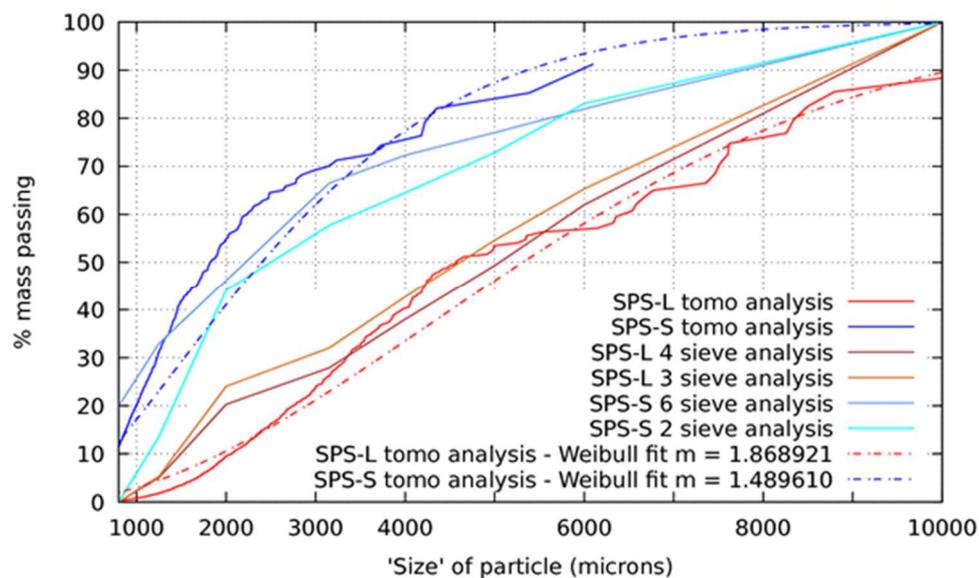

Fig. 11 Particle size distributions of post-mortem fragment sizes from sieving (SPS-L 4, SPS-L 3, SPS-S 6, SPS-S 2) (Rossiquet 2012) and tomography analysis (Forquin and Ando 2017). Comparison with Weibull and Rosin-Rammler distribution model fits

5   Discussion: role of the flaws population on the fragmentation process in ceramics

The edge-on impact experiments were numerically simulated considering the Denoual-Forquin-Hild anisotropic damage model (Denoual and Hild 2000; Forquin and Hild 2010). As observed in EOI tests, at high strain-rates, a large number of cracks initiates and propagates from existing defects resulting in a multiple fragmentation. The phenomenology of the fragmentation process can be explained in the following way: as the tensile stress increases at a specific loading rate, first cracks initiate from critical

(activated) defects. Their propagation through the loaded volume prevents the triggering of other critical defects in their vicinity. However, stress level continues to increase far from these growing "obscuration zones". The fragmentation process is analogous to a "competition" between stress increase in non-obscured zone and a sudden drop of loading in obscured zones. The concept of obscuration probability P_o (Denoual and Hild 2000; Forquin and Hild 2010) provides a representation of the part of the volume that is currently obscured by cracks already initiated on critical defects. The obscuration probability related to a multiple fragmentation process P_o reads:

$$P_o^{(i)}(T) = 1 - \exp\left(\int \frac{d\lambda_t(\sigma_i)}{dt} Z_o(T-t)dt\right) , \qquad \text{(Eq. 1)}$$

where λ_t is the density of critical defects related to the local principal stress component σ_i, $Z_o(T-t)$ is the obscured zone at the current time T due to a crack triggered at time t. By considering an obscuration zone growing in a self-similar way and assuming a constant crack speed ($V_{crack} = k.C$ with k a dimensionless parameter and C the 1D wave speed), the obscuration volume can be expressed as:

$$Z_o(T-t) = S[k.C(T-t)]^n , \qquad \text{(Eq. 2)}$$

S being a shape parameter ($4\pi/3$ if spherical obscuration volumes would be assumed), n being the dimension of the space considered ($n = 3$ in 3D). Considering a Weibull density of critical defects, λ_t is expressed as a power law function of the positive principal stress:

$$\lambda_t(\sigma_i) = \lambda_0 \left(\frac{\langle\sigma_i\rangle}{S_0}\right)^m , \qquad \text{(Eq. 3)}$$

where m is the Weibull modulus and $\lambda_0(S_0)^{-m}$ is the scale Weibull parameter deduced by averaging the tensile strength measured in quasi-static bending experiments according to:

$$\sigma_w = S_0\left(V_{eff}\lambda_0\right)^{-\frac{1}{m}} \Gamma\left(\frac{m+1}{m}\right) , \qquad \text{(Eq. 4)}$$

where Γ is the Eulerian integral of the second kind (gamma function) defined as:

$$\Gamma(1+x) = \int_0^\infty t^x \exp(-t)\, dt , \qquad \text{(Eq. 5)}$$

and V_{eff} is the effective volume of bending tests provided by (Davies 1973):

$$V_{eff} = \int_\Omega \left(\frac{<\sigma_I(\underline{x})>}{\sigma_m}\right)^m dv , \qquad \text{(Eq. 6)}$$

with $< \sigma_I(\underline{x}) >$ the positive part of the first principle stress at a given point of coordinates ($\underline{x}$) and σ_m its maximum value in the loaded volume. The obscuration probability can be expressed in differential form and implemented in an FE code according to:

$$\frac{d^{n-1}}{dt^{n-1}}\left(\frac{1}{1-P_o^{(i)}}\frac{dP_o^{(i)}}{dt}\right) = n!\, S(k.C)^n \lambda_t(\sigma_i) \quad \text{when} \quad \frac{d\sigma_i}{dt} > 0 \ \& \ \sigma_i > 0 . \qquad \text{(Eq. 7)}$$

Three macroscopic principle stress components Σ_i are computed as function of each obscuration probability variables $P_o^{(i)}$ and the microscopic strain components ε_i (Denoual and Hild 2000; Forquin and Hild 2010):

$$\overline{\Sigma} = \overline{\overline{K}}\left(E, v, P_o^{(i)}\right)\overline{\varepsilon} \quad \text{with} \quad \overline{\varepsilon} = \begin{bmatrix} \varepsilon_1 \\ \varepsilon_2 \\ \varepsilon_3 \end{bmatrix}, \ \overline{\Sigma} = \begin{bmatrix} \Sigma_1 \\ \Sigma_2 \\ \Sigma_3 \end{bmatrix} \quad \text{and} \quad \overline{\overline{K}}^{-1} = \frac{1}{E}\begin{bmatrix} \frac{1}{1-P_o^{(1)}} & -v & -v \\ -v & \frac{1}{1-P_o^{(2)}} & -v \\ -v & -v & \frac{1}{1-P_o^{(3)}} \end{bmatrix}, \quad \text{(Eq. 8)}$$

E and *v* being the Young's modulus and Poisson's ratio of the undamaged ceramic. If ones consider that the only critical defects located in non-obscured zones can be triggered, the crack density associated to each principal stress can be calculated by integrating the following differential equation:

$$\frac{d\lambda_{cracks}^{(i)}}{dt} = P_o^{(i)} \frac{d\lambda_t(\sigma_i)}{dt} \ . \tag{Eq. 9}$$

Therefore, the cracking density at any time *T* can be calculated as an output variable of the numerical simulation by integrating Eq. (9).

Table 2 Parameters of DFH model considered in the numerical simulation for the PS-S, SPS-S, PS-L and SPS-L SiC ceramics. Weibull parameters for the SPS-S, PS-L, SPS-L grades are provided from 4-point bending tests detailed in (Rossiquet, 2012). Weibull parameters for PS-S grade are deduced from data of 160 4-point bending tests provided by Saint-Gobain Research North America (NRDC) (Dargaud, 2021).

| Parameters:	PS-S	SPS-S	PS-L	SPS-L
Samples size (height x width x length) (mm³)	3 x 4 x 45	3 x 5 x 24		
Support and loading spans (mm)	40, 20	20.8, 10		
Weibull modulus, m	14.0	13.3	5.1	7.9
Effective volume, V_{eff} (mm³)	8.5	5.6	14.5	9.5
Mean tensile failure stress, $\sigma_w(V_{eff})$ (MPa)	406	388	306	440
Mean tensile failure stress for V_{eff} = 1 mm³ (MPa)	473	442	517	585
k	0.38			
Shape parameter, S	3.74			
1D wave speed, C_0 (m/s)	11 535			
Young's modulus (GPa)	410			
Poisson's ratio	0.14			
Density (Kg/m³)	3180			
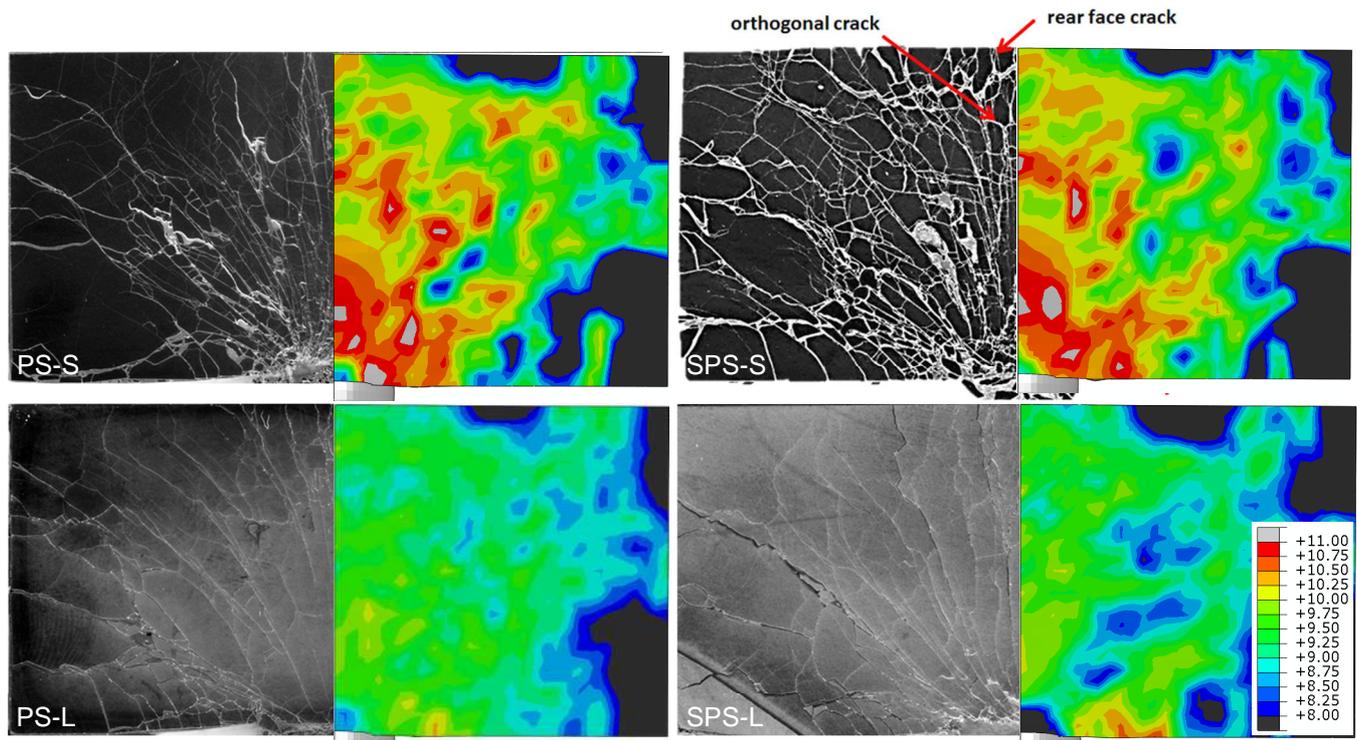
Fig. 12 Numerical simulation of the fragmentation process in PS-S, SPS-S, PS-L and SPS-L SiC ceramics subjected to EOI test (170 m/s) with DFH damage model. Isocontours of the final cracking density in log. scale (m^{-3}): for instance, λ = 9 would correspond to 10^9 cracks per m^3 or 1 crack per mm^3

A series of calculations are conducted with Abaqus Explicit Finite-Element code. The ceramic sample and the steel projectile are meshed with C3D8R elements (reduced integration) and the yield strength of the steel projectile is set to 1350 MPa. The striking velocity of the projectile is set to 170 m/s. The DFH anisotropic damage model is considered to model the ceramic target. The parameters considered in DFH model are reported in the Table 2. The Weibull parameters (Weibull modulus and scale Weibull parameter) were obtained from four-point bending tests. In the case of PS-S samples, the dimensions of the tested specimens were 3 x 4 x 45 mm3 (height x width x length) and the support and loading spans were 40 and 20 mm, whereas in the case of PS-L, SPS-S and SPS-L ceramics the tested samples were 3 x 5 x 24 mm3 (height x width x length) and the support and loading spans were 20.8 and 10 mm. The field of final cracking density (T = 7 μs) is illustrated in the Figure 12 for each SiC ceramics and is compared to the post-mortem cracking pattern (Fig. 9). The numerical simulation enables to explain the strong differences in cracking density visualized in the fragmented targets. Indeed, thanks to their lower Weibull modulus and higher average tensile strength, SPS-L and PS-L ceramics generate a lower number of cracks and larger fragments than the PS-S and SPS-S grades.

In addition, if ones assume a constant stress rate $\dot{\sigma}$, the final crack density (i.e. when the whole volume is obscured) is given by the following analytic expression which illustrates the influence of the Weibull parameters (first term), the loading rate (second term) and the parameters related to the size of obscuration volume (third term), (Denoual and Hild 2000; Forquin and Hild 2010):

$$\lambda_{cracks}^{T\to\infty} = \underbrace{\left(S_0\lambda_0^{-1/m}\right)^{\frac{-mn}{m+n}}}_{Crack\ inception} \underbrace{(\dot\sigma)^{\frac{mn}{m+n}}}_{Loading\ rate} \underbrace{\left(S^{1/n}k.C\right)^{\frac{-mn}{m+n}}}_{Crack\ propagation} \left(\frac{(m+n)!}{m!n!}\right)^{\frac{m}{m+n}} \Gamma\left(\frac{2m+n}{m+n}\right) , \quad \text{(Eq. 10)}$$

Now, if ones consider the same parameters (S, k and C) for each SiC microstructure and considering the strain-rate estimated in edge-on impact experiments at 10 mm from the impact point (7750 s^{-1} according to Fig. 6) the quasi-static mean failure stress (Y-axis) associated to a given crack density and an effective volume of 1 mm^3 can be calculated as function of the Weibull modulus (X-axis) by combining Equations (4) and (10):

$$\sigma_w = \frac{\dot\sigma}{kC.(S)^{\frac{1}{n}}.(V_{eff})^{\frac{1}{m}}.(\lambda_{cracks}^{T\to\infty})^{\frac{m+n}{mn}}} \Gamma\left(\frac{m+1}{m}\right)\Gamma\left(\frac{2m+n}{m+n}\right)^{\frac{m+n}{mn}}\left(\frac{(m+n)!}{m!n!}\right)^{\frac{1}{n}}. \quad \text{(Eq. 11)}$$

As illustrated in the graph of the Figure 13, the higher the quasi-static mean failure stress, the lower the final crack density. Conversely, the higher the Weibull modulus, the higher the final crack density. Finally, whereas the SPS-S and PS-S grades suffer from higher Weibull modulus and lower quasi-static tensile strength compared to others, the PS-L and SPS-L grades benefit from their low Weibull modulus and higher quasi-static tensile strength compared to SPS-S and PS-S grades. So, these predictions are consistent with the previous experimental findings (Figs. 8, 9, 10 and 11) and with the numerical results illustrated in the Figure 12.
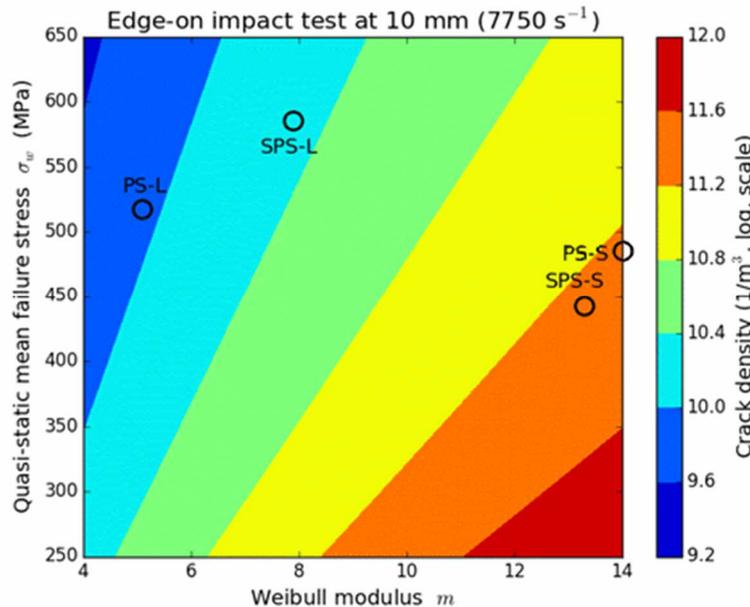
Fig. 13 Predictions of crack density with Eq. 7 as function of the quasi-static failure stress (V_{eff} = 1 mm^3) and the Weibull modulus considering a strain-rates of 7750/s and parameters of Table 2. The quasi-static failure stress (with V_{eff} = 1 mm^3) and the Weibull modulus for each SiC grade are also reported.

6 Conclusions

During the last three decades, the edge-on impact testing technique has been widely used to explore the fragmentation properties of different types of transparent and non-transparent ceramic grades. This technique presents strong advantages but also some limitations and drawbacks compared to other experimental techniques. Among the advantages, one may note that typical strain-rates ranging from few thousands of s^{-1} to a few tens of thousands of s^{-1} are generated leading to an intense multiple fragmentation process in the target. On the other hand, dynamic experiments conducted with Split Hokinson Pressure Bar apparatus are limited to much lower strain-rates (about a few tens to few hundreds of s^{-1}) when applied to ceramics, which leads to a single fracture in the tested specimen. In addition, in the so-called open configuration, the edge-on impact testing method provides the possibility to visualize the growth of fragmentation "in real time" by using high-speed photography with interframe time set in between 2 µs down to 0.1 µs. In addition, the fracture pattern can be analyzed with the so-called sarcophagus configuration by infiltrating the fragmented ceramic tile or by using a transparent sarcophagus to the visual light or to X-ray. These two types of analysis remain difficult to perform in the case of the spalling testing by plate-impact or by pulsed-power technology. Furthermore, the edge-on impact testing technique requires also much less costly equipment compared to pulsed power generator facilities or to the gas gun facilities that are used for plate-impact tests, which generally operate with a larger caliber and under vacuum. As main limitation, it can be observed that the edge-on impact testing configuration does not provide any direct strength measurement. The visualization of damage is usually restricted to the lateral surface in the case of non-transparent ceramic. In addition, the field of stress and stress-rate is non-uniformed, so a numerical analysis can be required to complement the experimental analysis.

In the present chapter, the properties of fragmentation process generated in four SiC ceramic grades with different microstructures under impact are compared. The edge-on impact tests conducted in the 'open configuration' and 'sarcophagus configuration' confirm that depending on the microstructures of SiC ceramics very different crack densities during and after impact are observed. The fragmentation pattern is also analyzed with X-ray micro-tomography CT scan analysis applied to two of the four grades, which confirm the strong differences in terms of cracking density and fragments size distribution.

Numerical simulations conducted with the DFH anisotropic damage model that is based on a description of the fragmentation process (i.e. initiation of cracks on non-obscured critical defects and obscuration of other critical defects due to release waves in the vicinity of propagating cracks) provide an explanation of the experimental result. Indeed, consistently with the experiments, much higher cracking densities are numerically predicted with the PS-S and SPS-S SiC ceramics compared to PS-L and SPS-L SiC grades when subjected to roughly the same impact loading conditions. The main difference being the Weibull parameters considered as input of the DFH model, it is concluded that the fragmentation process is mainly driven by the population of flaws from which cracks are triggered in the tested ceramic specimens. A quantitative comparison between the cracking patterns deduced from x-ray microtomography to the cracking density predictions provided by numerical modelling constitutes a prospect of this analysis.

Handbook of Damage Mechanics; Nano to Macro Scale for Materials and Structures

Second Edition

Disclosure: This manuscript is partly based on the following papers by the authors.

P. Forquin, J.-L. Zinszner, G. Rossiquet, B. Erzar, Microstructure influence on the fragmentation properties of dense silicon carbides under impact. Mech. Mater. 123, 59–76 (2018)

P. Forquin, E. Ando, Application of micro-tomography and image analysis to the quantification of fragmentation in ceramics after impact loading. Phil. Trans. R. Soc. A, 20160166 (2017).

P. Forquin, J.L. Zinszner, Experimental study of the dynamic fragmentation in transparent ceramic subjected to projectile impact, in Dynamic Behavior of Materials, ed. by D. Casem, L. Lamberson, J. Kimberley, vol. 1, (2017), pp. 165–170.

References

X. Brajer, P. Forquin, R. Gy, F. Hild, The role of surface and volume defects in the fracture of glass under quasi-static and dynamic loadings, J. Non-Crystalline Solids, 316, 42-53 (2003)

J. Cagnoux, J., A. Cosculluela, Influence of grain-size on triaxial dynamic behavior of alumina, in *Proceedings of the International Seminar on Dynamic Failure of materials : theory, experiments and numerics,* Technische Universität Wien, 2-4 Jan., pp73-84, Ed. By H.P. Rossmanith and A.J. Rosakis (1991)

W.W. Chen., A.M. Rajendran, B. Song, X. Nie, Dynamic fracture of ceramics in armor applications, J. Am. Ceram. Soc., 90(4), 1005–1018 (2007)

J.J. Chen, B.Q. Guo, H.B. Liu, H. Liu, P.W. Chen, Dynamic Brazilian Test of Brittle Materials Using the Split Hopkinson Pressure Bar and Digital Image Correlation Strain, 50, 563–570 (2014)

A. Cosculluela, Plasticité, endommagements et ruptures des alumines sous sollicitations dynamiques triaxiales : influence de la taille des grains (Ph.D. dissertation), University of Bordeaux, France (1992)

M. Dargaud, Experimental and numerical analysis of the failure modes induced in ceramic materials under dynamic loading. (Ph.D. dissertation), Université Grenoble Alpes, France, 2021

D.G.S. Davies, The Statistical Approach to Engineering Design in Ceramics, Proc. Brit. Ceram. Soc. 22, 429-452 (1973)

P.C. den Reijer, Impact on Ceramic Faced Armour (Ph.D. dissertation), Delft University of Technology, Netherlands (1991)

C. Denoual, F. Hild, A damage model for the dynamic fragmentation of brittle solids, Computer Methods in Applied Mechanics and Engineering, 183, 247-258 (2000)

Handbook of Damage Mechanics; Nano to Macro Scale for Materials and Structures

Second Edition

Y. Duplan, P. Forquin. Investigation of the multiple-fragmentation process and post-fragmentation behaviour of dense and nacre-like alumina ceramics by means of tandem impact experiments and tomographic analysis. Int. J. Impact Eng., 155, 103891 (2021). DOI: 10.1016/j.ijimpeng.2021.103891

P. Forquin, Endommagement et fissuration de matériaux fragiles sous impact balistique, rôle de la microstructure, (Ph.D. dissertation), Ecole Normale Supérieure de Cachan, France (2003)

P. Forquin, L. Tran, P-F. Louvigné, L. Rota, F. Hild, Effect of aluminum reinforcement on the dynamic fragmentation of SiC ceramics, Int. J. Impact Eng., 28, 1061-1076 (2003).

P. Forquin, L. Tran, P.-F. Louvigné, L. Rota, F. Hild, Effect of aluminum reinforcement on the dynamic fragmentation of SiC ceramics, Int. J. Impact Eng., 28, 1061-1076 (2003)

P. Forquin, M. Blasone, D. Georges, M. Dargaud. Continuous and discrete methods based on X-ray computed-tomography to model the fragmentation process in brittle solids over a wide range of strain-rates - application to three brittle materials. J. Mech. Physics Solids, 152, 104412 (2021). DOI: 10.1016/j.jmps.2021.104412

P. Forquin, F. Hild, A probabilistic damage model of the dynamic fragmentation process in brittle materials, Advances in Applied Mechanics, 44, 1-72 (2010)

P. Forquin, Experimental Investigation of the Dynamic Fragmentation Process in a Transparent Ceramic Under Impact Loading. In: Song B., Lamberson L., Casem D., Kimberley J. (eds) Dynamic Behavior of Materials, Volume 1, pp. 5-11, DOI: 10.1007/978-3-319-22452-7_2. Book series: Proceedings of the Society for Experimental Mechanics Series. Springer (2016)

P. Forquin J.L. Zinszner, Experimental Study of the Dynamic Fragmentation in Transparent Ceramic Subjected to Projectile Impact. In: Casem D., Lamberson L., Kimberley J. (eds) Dynamic Behavior of Materials, Volume 1, pp 165-170, DOI: 10.1007/978-3-319-41132-3_23. Book series: Proceedings of the Society for Experimental Mechanics Series. Springer (2017)

P. Forquin, E. Ando, Application of micro-tomography and image analysis to the quantification of fragmentation in ceramics after impact loading. Phil. Trans. R. Soc. A 20160166. DOI: 10.1098/rsta.2016.0166 (2017)

P. Forquin J.-L. Zinszner G. Rossiquet, B. Erzar, Microstructure influence on the fragmentation properties of dense silicon carbides under impact. Mechanics of Materials. 123, 59-76 (2018)

F. Galvez, J. Rodriguez, V. Sanchez, Tensile Strength Measurements of Ceramic Materials at High Rates of Strain. J. Physique IV 7(C3), 151-156 (1997)

B.-K. Jeon, J.-H. Jang, K.-S. Hong, Robust region segmentation based on a pseudo-distance map. Journal of Electronic Imaging 13(3), 602–612 (2004)

Handbook of Damage Mechanics; Nano to Macro Scale for Materials and Structures

Second Edition

A. Krell, E. Strassburger. Order of influences on the ballistic resistance of armor ceramics and single crystals. Materials Science and Engineering: A, 597, 422–430 (2014)

R.B. Leavy, J.D. Clayton, O.E. Strack, R.M. Brannon, E. Strassburger, Edge on Impact Simulations and Experiments, Procedia Engineering, 58, 445–452 (2013)

J.W. McCauley, E. Strassburger, P. Patel, B. Paliwal, K.T. Ramesh, Experimental Observations on Dynamic Response of Selected Transparent Armor Materials. Exp. Mech. 53(1), 3–29 (2013)

M. Normandia, J. Lasalvia, W. Gooch, J.W. Rajendran, A.M. Rajendran, Protecting the Future Force: Ceramics Research Leads to Improved Armor Performance. AMMTIAC, New York (2004)

W. Riedel, S. Hiermaier, K. Thoma, Transient stress and failure analysis of impact experiments with ceramics, Materials Science and Engineering B, 173, 139–147 (2010)

P. Riou, Contribution à l'étude de l'endommagement du Carbure de Silicium lors d'un impact de basse énergie : application aux blindages, (Ph.D. dissertation), Ecole Nationale Supérieure des Mines de Paris (1996)

P. Riou, C. Denoual, C.E. Cottenot, Visualization of the damage evolution in impacted silicon carbide ceramics, Int. J. Impact Eng., 21 (4), 225-235 (1998)a

P. Riou, C.E. Cottenot, M. Boussuge, Anisotropic damage model for impacted ceramic material; application to silicon carbide. Int. J. Impact Eng., 21(8), 683-693 (1998)

G. Rossiquet, Carbure de silicium pour application blindage : élaboration et étude du comportement à l'impact, (Ph.D. dissertation), Université de Bourgogne, France (2012)

M. Scapin L. Peroni M. Avalle, Dynamic Brazilian Test for Mechanical Characterization of Ceramic Ballistic Protection. Hindawi, Shock and Vibration, Vol. 2017, Article ID 7485856 (2017)

H. Senf, E. Strassburger, H. Rothenhäusler, Stress wave induced damage and fracture in impacted glasses, J. Phys. IV France, 04, C8-741-C8-746, DOI: 10.1051/jp4:19948114 (1994)

E. Strassburger, H. Senf, Experimental Investigations of Wave and Fracture Phenomena in Impacted Ceramics and Glasses. ARL-CR-214, Army Research Laboratory (1995)

E. Strassburger, Visualization of impact damage in ceramics using the edge-on impact technique, Int. J. Appl. Ceram. Technol. 1(3), 235–242 (2004)

E. Strassburger, M. Hunzinger, P. Patel, J.W. McCauley, Analysis of the fragmentation of AlON and Spinel under ballistic impact, J. Appl. Mech. 80, 031807 (2013)

Handbook of Damage Mechanics; Nano to Macro Scale for Materials and Structures

Second Edition

E. Strassburger, P. Patel, J.-W. McCauley, D.W. Templeton, W. Douglas, Visualization of wave propagation and impact damage in a polycrystalline transparent ceramic–ALON, In: 22nd Int. Symposium on Ballistics (2005)

E. Strassburger, P. Patel, J.-W. McCauley, D.W. Templeton, High speed photographic study of wave propagation and impact damage in fused silica and ALON using the edge-on impact EOI method. AIP Conf. Proc. 845(II), 892–895 (2006)

A.L. Tonge, K.T. Ramesh, Multi-scale defect interactions in high-rate brittle material failure. Part I: Model formulation and application to ALON, J. Mech. Physics Solids, 86, 117–149 (2016)

G. Zhang, G.A. Gazonas, F. Bobaru, Supershear damage propagation and sub-Rayleigh crack growth from edge-on impact: A peridynamic analysis, Int. J. Impact Eng. 113, 73–87 (2018)

J.-L. Zinszner, Identification des paramètres matériau gouvernant les performances de céramiques à blindage, (Ph.D. dissertation), Université de Lorraine, France (2014)

J.-L. Zinszner, B. Erzar, P. Forquin, Strain-rate sensitivity of the tensile strength of two silicon carbides: experimental evidence and micromechanical modelling, Phil. Trans. R. Soc., A 20160167. DOI: 10.1098/rsta.2016.0167 (2017)

J.-L. Zinszner, B. Erzar, P. Forquin, E. Buzaud, Dynamic fragmentation of an alumina ceramic subjected to shockless spalling: an experimental and numerical study, J. Mech. Phys. Solids, 85, 112–127 (2015)

J.-L. Zinszner, P. Forquin, G. Rossiquet, Experimental and numerical analysis of the dynamic fragmentation in a SiC ceramic under impact, Int. J. Impac Eng., 76, 9-19 (2015)

Index Terms

Crack density

Dynamic fragmentation

Edge-On-Impact

Obscuration

Silicon Carbide

Handbook of Damage Mechanics; Nano to Macro Scale for Materials and Structures

Second Edition

Table des matières

Figures:

Handbook of Damage Mechanics; Nano to Macro Scale for Materials and Structures

Second Edition

Tables: